Monthly Notices
of the
ROYAL ASTRONOMICAL SOCIETY

MNRAS **456,** L89–L93 (2016) doi:10.1093/mnrasl/slv184

Polycyclic aromatic hydrocarbons and molecular hydrogen in oxygen-rich planetary nebulae: the case of NGC 6720

N. L. J. Cox,[1,2]★ P. Pilleri,[1,2]★ O. Berné,[1,2] J. Cernicharo[3] and C. Joblin[1,2]

[1]*Université de Toulouse, UPS-OMP, IRAP, F-31028 Toulouse, France*
[2]*CNRS, IRAP, 9 Av. colonel Roche, BP 44346, F-31028 Toulouse, France*
[3]*Group of Molecular Astrophysics, ICMM, CSIC, C/Sor Juana Inés de La Cruz N3, E-28049 Madrid, Spain*

Accepted 2015 November 13. Received 2015 November 13; in original form 2015 August 31

ABSTRACT

Evolved stars are primary sources for the formation of polycyclic aromatic hydrocarbons (PAHs) and dust grains. Their circumstellar chemistry is usually designated as either oxygen rich or carbon rich, although dual-dust chemistry objects, whose infrared spectra reveal both silicate- and carbon-dust features, are also known. The exact origin and nature of this dual-dust chemistry is not yet understood. *Spitzer*–Infrared Spectrograph (IRS) mid-infrared spectroscopic imaging of the nearby, oxygen-rich planetary nebula NGC 6720 reveals the presence of the 11.3 μm aromatic (PAH) emission band. It is attributed to emission from neutral PAHs, since no band is observed in the 7–8 μm range. The spatial distribution of PAHs is found to closely follow that of the warm clumpy molecular hydrogen emission. Emission from both neutral PAHs and warm H_2 is likely to arise from photodissociation regions associated with dense knots that are located within the main ring. The presence of PAHs together with the previously derived high abundance of free carbon (relative to CO) suggest that the local conditions in an oxygen-rich environment can also become conducive to *in situ* formation of large carbonaceous molecules, such as PAHs, through a bottom-up chemical pathway. In this scenario, the same stellar source can enrich the interstellar medium with both oxygen-rich dust and large carbonaceous molecules.

Key words: H II regions – planetary nebulae: individual: NGC 6720 – infrared: stars.

1 INTRODUCTION

The asymptotic giant branch (AGB) and planetary nebula (PN) phases of stellar evolution govern the chemical enrichment of the interstellar medium (ISM) by low- to intermediate-mass stars. Evolved stars are efficient dust factories, but the processes involved in dust formation and evolution are still shrouded in mystery. Unlike molecules, dust grains can only be efficiently formed in the innermost warm regions of evolved stars (Gail & Sedlmayr 1988). Carbon-rich evolved stars are formation sites of polycyclic aromatic hydrocarbons (PAHs). Bottom-up formation is either via pyrolysis (Frenklach & Feigelson 1989; Cherchneff, Barker & Tielens 1992) or photolysis (Cernicharo 2004). The top-down process could occur through shock-, photo, or chemical destruction of carbonaceous or SiC grains (Jones, Tielens & Hollenbach 1996; Pilleri et al. 2012; Merino et al. 2014).

Generally, silicate dust formation is related to oxygen/O-rich winds (C/O < 1), while carbonaceous dust formation occurs primarily in carbon/C-rich winds (C/O > 1). PAH features are present in planetary nebulae (PNe) with C/O abundance ratios as low as ∼0.6 (Cohen & Barlow 2005; Delgado-Inglada & Rodríguez 2014). However, in several cases both oxygen-rich and carbon-rich dust features are seen in (spatially integrated) infrared spectra of PNe (e.g. Cerrigone et al. 2009; Perea-Calderón et al. 2009). García-Rojas et al. (2013) found that dual-dust chemistry in PNe with O-rich nebulae show weak PAH bands and crystalline/amorphous silicates, while the C-rich ones have strong PAH bands and very weak crystalline silicate features. García-Hernández & Górny (2014) identified the presence of dual-dust chemistry in PNe mainly with high-metallicity and relatively high-mass (∼3–5 $M_\odot$) young PNe. Dual-dust chemistry in C-rich PNe has been explained in terms of different evolutionary phases. The silicate dust emission is formed earlier. PAHs are formed in a later mass-loss phase and are present in the outflows (Matsuura et al. 2004).

For PAHs observed in O-rich Galactic bulge PNe (Perea-Calderón et al. 2009; Guzman-Ramirez et al. 2011, 2014), this scenario seems less satisfactory since these PNe are mostly old, low-mass stars that are not expected to go through a third dredge-up phase, and therefore show no enhanced C/O ratios. An alternative explanation is that PAHs in these objects are formed *in situ* in an UV-irradiated dense torus as suggested by Matsuura et al. (2004) and Cernicharo (2004). In this scenario, PAHs form in a region just outside where some UV photons penetrate and dissociate CO and the free

★ E-mail: nick.cox@irap.omp.eu (NLJC); paolo.pilleri@irap.omp.eu (PP)

carbon can subsequently aggregate there and lead to formation of PAHs (e.g. Matsuura et al. 2004). Cernicharo (2004) has shown that in dense Photo-dissociation regions (PDRs) of proto-PNe, the photodissociation of CO and other species leads to the growth of carbon chains, and to the production of carbon clusters. This rich photochemistry suggests a possible bottom-up scenario for the formation of PAHs. Agúndez, Cernicharo & Goicoechea (2008) have shown that the same applies to O-rich environments as those found in protoplanetary discs where C_2H_2 and HCN are found with very high abundances.

In this Letter, we present *Spitzer* spectroscopy of the nearby PN NGC 6720 (Ring Nebula). Section 2 presents the *Spitzer* observations of NGC 6720. The results we obtained for the PAH and H_2 emission are discussed in Section 3 and put in perspective in Section 4.

2 SPECTROSCOPIC IMAGING OF NGC 6720

NGC 6720 is a nearby (740^{+400}_{-200} pc; O'Dell, Henney & Sabbadin 2009), oxygen-rich bipolar PN. Its main ring corresponds to an ionization-bounded torus structure seen nearly pole-on with lobes directed along the line of sight (cf. O'Dell et al. 2013a). The central star of the PN (CSPN) has an effective temperature of $T_{\rm eff}$ = 120 000 K and a stellar luminosity $L_\star = 200\,{\rm L}_\odot$ (O'Dell, Sabbadin & Henney 2007). The reported C/O abundance ratio ranges from 0.4 to 1.0 (Delgado-Inglada & Rodríguez 2014).

NGC 6720 has been observed with the *Spitzer* Space Telescope (Werner et al. 2004) as part of programme 40536 (PI: H. Dinerstein). The Infrared Spectrograph (IRS) SH observations (Houck et al. 2004) have been processed with CUBISM (Smith et al. 2007), including sky background subtraction and 3σ clipping. The 3D spectral data cube allows us to study the mid-infrared spectrum (10–19.6 μm, $R \sim 600$) of NGC 6720 in a region of 99 × 18 arcsec with a plate scale of 1.8 arcsec per pixel, as shown in Fig. 1.

In an initial assessment, we extracted two (average) spectra, one towards the central star and one pertaining to the main dust ring. The extracted spectra are shown in Fig. 2. Both spectra clearly differ in terms of relative strength of the gas emission lines. All the gas emission lines typically detected between 10 and 20 μm for PNe are present in NGC 6720. Most noticeable, however, is the presence of the 11.3 μm PAH band. The 12.0 and 12.7 μm PAH bands are also detected in the spectrum for the main ring, confirming the presence of PAHs. The presence of the 11.3 μm PAH band is further corroborated by lower sensitivity IRS SH spectra (calibration programme 1424) taken at two positions (N–S) on the ring perpendicular to the data cube (E–W). Previously, PAH emission bands were thought to be absent in this PN, although in hindsight the 11.3 μm band (contaminated by a H I line) is tentatively seen in the *Spitzer*-SL spectra shown by Hora et al. (2009).

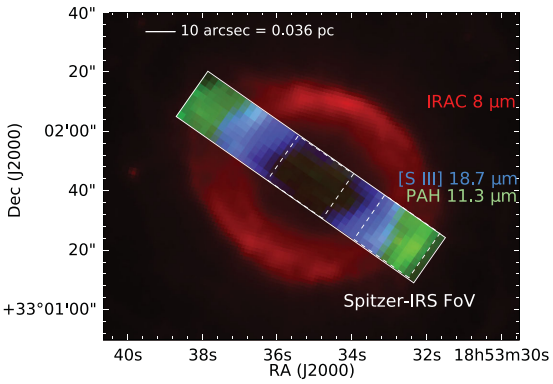

Figure 1. *Spitzer*–IRS maps of the 11.3 μm emission feature (green) and the [S III] emission line (blue) in the Ring Nebula overlaid on top of the *Spitzer* IRAC 8 μm image (red). The two white squares (dashed lines) indicate the extraction region for the spectra shown in Fig. 2.

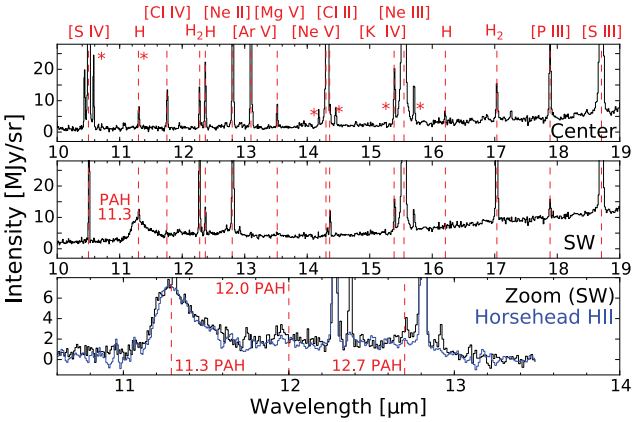

Figure 2. *Spitzer*–IRS SH spectra extracted from the 3D spectral-cube at two positions in the Ring Nebula. The positions are indicated by the two white-dashed squares in Fig. 1. The top panel shows a spectrum from the central hot-gas cavity and the middle panel shows the spectrum 'SW' arising from the main dust ring. Emission lines arising from several atoms and molecular hydrogen are labelled (ghost lines are indicated with asterisks). The bottom panel shows a close-up view of the (continuum subtracted) 11–13 μm PAH emission complex. The PAH emission spectrum of the Horsehead H II region (Compiègne et al. 2007), scaled by a factor of 0.4 to match the 11.3 μm peak intensity, is shown for reference.

No clear detection of a PAH feature in the 7–8 μm range could be obtained; The data are very noisy and suffer from a bad overlap between the two SL modules of the IRS spectrograph. Previous spectra obtained with ISOCAM Circular Variable Filters (CVF) have insufficient spectral resolution and sensitivity to detect PAH bands in the presence of strong atomic emission lines. The ISO-Short Wavelength Spectrometer (SWS) aperture does not cover the main ring. *Spitzer* LH/LL (20–40 μm) spectroscopy (programme 1424) of the dust ring is of insufficient sensitivity and spectral resolution to discern the presence of any dust features.

Line intensities for a representative subset of species are extracted from the *Spitzer* spectrum for each position in the spectral map. This set of lines traces roughly the ionizing radiation field throughout the nebula, that corresponds to the photon energies (∼13–60 eV) required to bring atoms in a certain ionization state. The spatial distribution of the mid-infrared H_2 S(1) and S(2) emission lines at 17.04 and 12.28 μm, and the 11.3 μm PAH band is shown in Fig. 3.

3 DISCUSSION

Fig. 4 reveals a close relation between the radial distributions of PAH, H_2, and dust emission in NGC 6720 (see van Hoof et al. 2010 for a comparative study between H_2 and dust emission). The co-spatial distribution of H_2 and PAH emission shows that both species are present and excited at similar locations within the molecular ring. PAHs could also be involved in the formation of H_2 (Habart et al. 2003; Boschman et al. 2015). Next, we discuss the observed PAH bands (Section 3.1) and give a brief analysis of the H_2 emission (Section 3.2). Section 3.3 then examines these results in the context of hydrocarbon photochemistry.

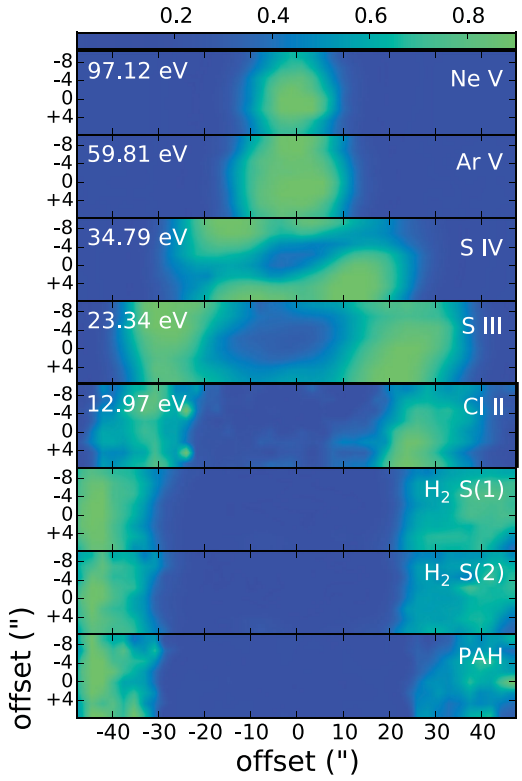

Figure 3. 2D spatial distribution of line intensity for the atomic (Ne V, Ar V, S IV, S III, Cl II) and molecular (H_2, PAH) tracers in NGC 6720. Intensities are normalized to the maximum value found for each species. Negative offsets are towards the south-west. The atomic species and the energies (eV) required to bring them in the specified ionization state are indicated.

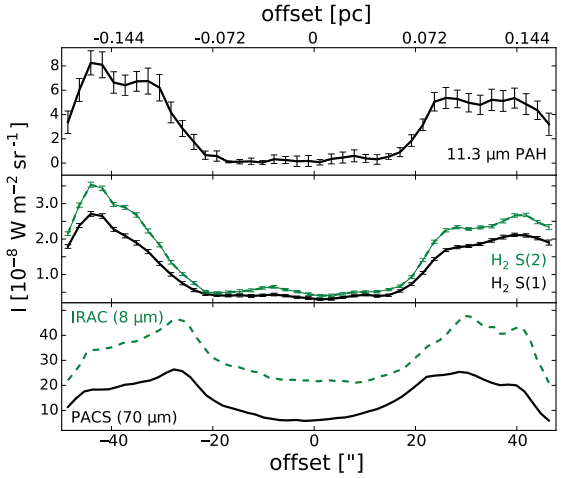

Figure 4. Radial profiles for PAH and H_2 integrated intensities, and infrared (dust) emission at 8 and 70 μm (W m^{-2} sr^{-1}).

3.1 PAH emission bands: profile and intensity

The 11.3 μm PAH band is observed at the position of 11.26 ± 0.05 μm, which is typical for that band (Hony et al. 2001). The full width at half-maximum is ∼0.33 μm. This is larger than typical, and is due to a red wing extending up to ∼11.6 μm. The total integrated emission of the 11.3 μm feature in the main ring ranges from ∼2 to 8×10^{-8} W m^{-2} sr^{-1}. For the PAH bands extracted from the 'SW' region (Fig. 2), the peak intensity is ∼7 MJy sr^{-1} with an integrated line intensity of 6.7×10^{-8} W m^{-2} sr^{-1}. I(11.3 μm), normalized by the total integrated infrared emission (TIR), is consistent with the relation with C/O ratio as derived by Cohen & Barlow (2005) for a large sample of PNe with C/O ≈ 0.3–3. The integrated line intensities of the 12.0 and 12.7 μm PAH bands in the 'SW' region are estimated to be 2.1 ± 0.3 and 2.2 ± 0.7 × 10^{-8} W m^{-2} sr^{-1}, respectively. The 7.7 μm PAH feature is not detected (Section 2). We derive an upper limit of its peak intensity, $I(7.7) = 0.3 \pm 1.3$ MJy sr^{-1}, to be compared to $I(11.3) = 7.0 \pm 0.82$ MJy sr^{-1}.

Pech, Joblin & Boissel (2002) modelled the emission of a distribution of PAHs in IRAS 21282+5050 suggesting that the extended profile of the 11.3 μm band is due to the smallest sizes of the PAH distribution (containing between 30 and 48 carbon atoms). Candian & Sarre (2015) also modelled the 11.3 μm emission band with neutral PAHs. These authors conclude that a profile with a peak at a relatively longer wavelength and with a more extended red tail (as well as a less steep short wavelength side) implies that lower mass PAHs are relatively more abundant. Hony et al. (2001) argue that the $I(12.7)/I(11.3)$ band strength ratio is determined by molecular structure, with low values associated with (compact) PAHs present in PNe. The $I(7.7)/I(11.3)$ ratio is < 0.26 which is below the values determined by Pilleri et al. (2012) for PAH and PAH^+ template spectra, which are 0.56 and 2.77, respectively. Although such a low value is rather exceptional, quantum chemistry calculations indicate that it is possible for neutral PAHs (Langhoff 1996; see Pauzat 2011 for a review) and even for very large ones (Bauschlicher, Peeters & Allamandola 2008; Ricca et al. 2012).

Ionized PAHs are expected to dominate in PDRs with large values of $G_0/n_e > 10^4$ (where G_0 is the radiation field strength in Habing units of 1.6 10^{-6} W m^{-2}), whereas mostly neutral PAHs or even negatively charged PAHs are expected to be found in PNe and H II regions when the medium is fully ionized ($n_e \sim n_H$) and low values of $G_0/n_e < 10^3$ prevail (Joblin et al. 2008). For the ring of NGC 6720 the effective G_0 is ≈200–400.[1] A predominance of neutral PAHs has previously been reported for the Horsehead nebula H II region, where $G_0 \sim 100$ (Compiègne et al. 2007). In this case, the usually strong 6.2 and 7.7 μm PAH bands are also absent, whereas the 11–13 μm PAH emission spectrum is very similar to that of NGC 6720 (Fig. 2, bottom panel; Compiègne et al. 2007). Similar profiles are also seen in the PNe IRAS 21282+5050 and IRAS 17047−5650 (Hony et al. 2001) and mixed-chemistry post-AGB star IRAS 16279−4756 (Matsuura et al. 2004).

3.2 H_2 temperature and density

The presence of H_2 in PNe is attributed to PDRs associated with the dense knots residing in the ionized regions (Speck et al. 2003; Manchado et al. 2015). Aleman & Gruenwald (2011) find that H_2 infrared emission lines in PNe are produced mainly in the warm and partially ionized transition zone between the ionized H II region and the neutral PDR. Additional heating and ionization of the gas is required to explain the strong H_2 emission lines. Possible mechanisms are soft X-rays from the hot CSPN (Natta & Hollenbach 1998; Vicini et al. 1999; Aleman & Gruenwald 2011; though no diffuse X-ray emission is observed; Kastner et al. 2012), shocks

[1] From the combined *Herschel*-PACS (van Hoof et al. 2010) and *Spitzer*-LH dust emission, the total integrated infrared dust emission, TIR ≈ 2.0 × 10^{-5} W m^{-2} sr^{-1}, is a tracer of the energy input: G_0(TIR) = 4π × TIR / (1.6 × 10^{-6}) ≈180. Alternatively the radiation field strength at 0.1 pc from the central star can be estimated as from an on-the-spot approximation, $G_0 = 625\, L_\star \chi/(4\pi d^2) = 402$ (Tielens 2005, p. 319).

(Arias et al. 2001), or the development of an extreme-UV-dominated advective PDR in which the ionization and dissociation fronts have merged (Henney et al. 2007).

The integrated line strengths for the H_2(0-0) S(1) and S(2) emission from the main ring range from 1 to 3 $\times$ 10^{-8} W m^{-2} sr^{-1} (Fig. 4). In addition, we extracted H_2 S(1) to S(4) integrated line intensities from a small region in the north–east part of the ring for which a single (lower resolution) *Spitzer*-SL spectrum is available. Assuming thermal equilibrium we use the line intensities to derive the rotational temperature and column density of H_2: $T(H_2) = 620^{+121}_{-87}$ K, $N(H_2) = 1.0^{+0.6}_{-0.4} \times 10^{18}$ cm^{-2}. These values are comparable to those derived by Cox et al. (1998) for the Helix Nebula: $T(H_2) = 900$ K and $N(H_2) = 2.0 \times 10^{18}$ cm^{-2}.

The H II region drives a shock in the globule and hence the pressure in the external molecular shell around the globule (where H_2 is emitting) will be comparable to the pressure in the H II region (e.g. Bertoldi 1989). Pressure equilibrium at the ionization front is given by $2\, n_e\, T_e = n_H\, T_{\rm gas}$. If photoevaporation occurs, this provides a lower density limit. Assuming that the H_2 rotational temperature we derived above is an upper limit to the gas kinetic temperature (i.e. $v = 0$ rotational levels are excited by collisions but also by UV fluorescence cascades in the surface PDR of the globules), as well as $T_e = 10\,500 \pm 1000$ K (Liu et al. 2004) and $n_e = 400 \pm 200$ cm^{-3} (O'Dell et al. 2013b), we obtain $n_H >$ 1–2.5 $\times$ 10^4 cm^{-3}. This is consistent with estimates from optical studies (O'Dell et al. 2002).

The gradual increase of H_2 intensity from 0.07 to 0.14 pc is linked to the decrease of the H_2 destruction rate with the attenuation of UV photons (corresponding to $A_V \approx 0.5$; Pilleri et al. 2012), while the sharp increase of PAH intensity at ∼0.08 pc is primarily due to a density gradient (PAHs are less sensitive to destruction by UV photons than H_2). $A_V = 0.5$ mag corresponds to N(H)∼ 10^{21} cm^{-2}, which yields an average volume density of 10^4 cm^{-3}, with higher densities inside the knots.

3.3 Hydrocarbon photochemistry

We expand here on the scenario proposed by e.g. Matsuura et al. (2004), Cernicharo (2004), and Guzman-Ramirez et al. (2011) in which CO is dissociated and PAHs are formed from free carbon. In the case of NGC 6720, the abundance of elemental carbon (i.e. C and C^+) is an order of magnitude higher than that of CO (Bachiller et al. 1994; Sahai et al. 2012), likely a result of dissociation of the latter by the strong radiation field of the high-excitation CSPN. Both CO- and C-emitting regions are clumped. As shown in the previous section, these clumps have high density ($>10^4$ cm^{-3}) and are exposed to a moderate radiation field ($G_0 \sim 200$). Cernicharo (2004) and Agúndez et al. (2008) have included in their chemical models for C- and O-rich environments reactions such as $C_2 + H_2 \rightarrow C_2H + H$, $C_2H + H_2 \rightarrow C_2H_2 + H$, and $C^+ + H_2 = CH^+ + H$ which have moderate activation barriers, which make them very slow in the cold ISM, but become rapid enough to control the abundance of C-bearing species at the high temperatures and high H_2 densities prevailing in the PDRs of (proto-)PNe. This is because chemical reactions involving H_2 v= 0 with radicals in a warm gas become significantly efficient if the volume density is large enough (Cernicharo 2004). H_2 v=1 reactions with more complex organic molecules could also overcome activation barriers of several thousand Kelvin allowing the growth of chemical complexity. In a C-rich PDR environment, C_2H_2 and HCN play a key role in the photochemistry (Cernicharo 2004), while for O-rich environments Agúndez et al. (2008) have shown that the photodissociation of CO and N_2 provide the path to the formation of C_2H_2 and HCN with abundances similar to those of C-rich environments. The high (H_2) gas temperature, together with freely available C, suggests a very fast and rich photochemistry at the surface of the dense knots existing in the main ring of NGC 6720. Together, these conditions favour a bottom-up formation of large carbonaceous molecules.

It is not clear how this process would give rise to a peculiar PAH population such as observed for NGC 6720. The PAH size distribution will be the result of the equilibrium between formation and destruction, where UV destruction generally favours increased abundance of large PAHs which are more stable (Montillaud, Joblin & Toublanc 2013). Although the large PAHs have high probability to be ionized rather than photodissociated (Zhen et al. 2015), the high electron abundance provides a competing recombination rate, which shifts the balance in favour of neutral PAHs.

4 SUMMARY AND CONCLUSIONS

We present the unexpected detection of a weak 11.3 μm PAH emission band in the main dust torus of O-rich PN NGC 6720. The band profile (position and red wing) and the absence of noticeable bands in the 7–8 μm range indicates that the emitting population consists primarily of neutral PAHs and contains a relatively higher abundance of smaller specie as found in most other objects. The spatial distribution of PAHs is closely correlated with the clumpy distribution of H_2 revealing the presence of PDRs associated with dense knots exposed to a moderate radiation field. For the physical environment associated with dense knots inside an ionized region, chemical models provide a way to transform a gas dominated by H_2, CO, H_2O, N_2 with C/O < 1 into a gas where complex carbon chemistry can occur and this might provide a pathway to form PAHs through a bottom-up process. In NGC 6720, reactions with large activation barriers could be facilitated by excitation of H_2 in v=1. A more detailed inventory of the properties and chemistry of nebular knots in oxygen-rich PNe will require observations at higher angular resolution. Regardless of the exact formation mechanism involved, our analysis indicates that complex hydrocarbon chemistry, including the formation of large molecules (with more than 30 C atoms), can occur in PDRs associated with high-density knots located within the ionized regions of O-rich PNe. Therefore, if knots are commonly formed in (old) O-rich PNe, these can enrich the ISM also with carbonaceous material.

ACKNOWLEDGEMENTS

We acknowledge helpful comments by the referee. The research leading to these results has received funding from the European Research Council under the European Union's Seventh Framework Programme (FP/2007-2013) ERC-2013-SyG, Grant Agreement No. 610256 NANOCOSMOS. PP acknowledges financial support from the Centre National Etudes Spatiales (CNES). The IRS was a collaborative venture between Cornell University and Ball Aerospace Corporation funded by NASA through the Jet Propulsion Laboratory and Ames Research Centre.

REFERENCES

Agúndez M., Cernicharo J., Goicoechea J. R., 2008, A&A, 483, 831
Aleman I., Gruenwald R., 2011, A&A, 528, A74
Arias L., Rosado M., Salas L., Cruz-González I., 2001, AJ, 122, 3293
Bachiller R., Huggins P. J., Cox P., Forveille T., 1994, A&A, 281, L93
Bauschlicher C. W., Jr, Peeters E., Allamandola L. J., 2008, ApJ, 678, 316
Bertoldi F., 1989, ApJ, 346, 735

Boschman L., Cazaux S., Spaans M., Hoekstra R., Schlathölter T., 2015, A&A, 579, A72
Candian A., Sarre P. J., 2015, MNRAS, 448, 2960
Cernicharo J., 2004, ApJ, 608, L41
Cerrigone L., Hora J. L., Umana G., Trigilio C., 2009, ApJ, 703, 585
Cherchneff I., Barker J. R., Tielens A. G. G. M., 1992, ApJ, 401, 269
Cohen M., Barlow M. J., 2005, MNRAS, 362, 1199
Compiègne M., Abergel A., Verstraete L., Reach W. T., Habart E., Smith J. D., Boulanger F., Joblin C., 2007, A&A, 471, 205
Cox P. et al., 1998, ApJ, 495, L23
Delgado-Inglada G., Rodríguez M., 2014, ApJ, 784, 173
Frenklach M., Feigelson E. D., 1989, ApJ, 341, 372
Gail H.-P., Sedlmayr E., 1988, A&A, 206, 153
García-Hernández D. A., Górny S. K., 2014, A&A, 567, A12
García-Rojas J., Peña M., Morisset C., Delgado-Inglada G., Mesa-Delgado A., Ruiz M. T., 2013, A&A, 558, A122
Guzman-Ramirez L., Zijlstra A. A., Níchuimín R., Gesicki K., Lagadec E., Millar T. J., Woods P. M., 2011, MNRAS, 414, 1667
Guzman-Ramirez L., Lagadec E., Jones D., Zijlstra A. A., Gesicki K., 2014, MNRAS, 441, 364
Habart E., Boulanger F., Verstraete L., Pineau des Forêts G., Falgarone E., Abergel A., 2003, A&A, 397, 623
Henney W. J., Williams R. J. R., Ferland G. J., Shaw G., O'Dell C. R., 2007, ApJ, 671, L137
Hony S., Van Kerckhoven C., Peeters E., Tielens A. G. G. M., Hudgins D. M., Allamandola L. J., 2001, A&A, 370, 1030
Hora J. L., Marengo M., Smith H. A., Cerrigone L., Latter W. B., 2009, in Sheth K., Noriega-Crespo A., Ingalls J., Paladini R., eds, The Evolving ISM in the Milky Way and Nearby Galaxies. p. 29, preprint (arXiv:0803.3937)
Houck J. R. et al., 2004, ApJS, 154, 18
Joblin C., Szczerba R., Berné O., Szyszka C., 2008, A&A, 490, 189
Jones A. P., Tielens A. G. G. M., Hollenbach D. J., 1996, ApJ, 469, 740
Kastner J. H. et al., 2012, AJ, 144, 58
Langhoff S. R., 1996, J. Phys. Chem., 100, 2819
Liu Y., Liu X.-W., Barlow M. J., Luo S.-G., 2004, MNRAS, 353, 1251
Manchado A., Stanghellini L., Villaver E., García-Segura G., Shaw R. A., García-Hernández D. A., 2015, ApJ, 808, 115
Matsuura M. et al., 2004, ApJ, 604, 791
Merino P. et al., 2014, Nat. Commun., 5, 3054
Montillaud J., Joblin C., Toublanc D., 2013, A&A, 552, A15
Natta A., Hollenbach D., 1998, A&A, 337, 517
O'Dell C. R., Balick B., Hajian A. R., Henney W. J., Burkert A., 2002, AJ, 123, 3329
O'Dell C. R., Sabbadin F., Henney W. J., 2007, AJ, 134, 1679
O'Dell C. R., Henney W. J., Sabbadin F., 2009, AJ, 137, 3815
O'Dell C. R., Ferland G. J., Henney W. J., Peimbert M., 2013a, AJ, 145, 92
O'Dell C. R., Ferland G. J., Henney W. J., Peimbert M., 2013b, AJ, 145, 93
Pauzat F., 2011, in Joblin C., Tielens A. G. G. M., eds, EAS Publ. Ser. Vol. 46, Computational IR Spectroscopy for PAHs: From the Early Years to the Present Status. EAS Publications Series, Toulouse, France, p. 75
Pech C., Joblin C., Boissel P., 2002, A&A, 388, 639
Perea-Calderón J. V., García-Hernández D. A., García-Lario P., Szczerba R., Bobrowsky M., 2009, A&A, 495, L5
Pilleri P., Montillaud J., Berné O., Joblin C., 2012, A&A, 542, A69
Ricca A., Bauschlicher C. W., Jr, Boersma C., Tielens A. G. G. M., Allamandola L. J., 2012, ApJ, 754, 75
Sahai R., Morris M. R., Werner M. W., Güsten R., Wiesemeyer H., Sandell G., 2012, A&A, 542, L20
Smith J. D. T. et al., 2007, PASP, 119, 1133
Speck A. K., Meixner M., Jacoby G. H., Knezek P. M., 2003, PASP, 115, 170
Tielens A. G. G. M., 2005, The Physics and Chemistry of the Interstellar Medium. Cambridge Univ. Press, Cambridge
van Hoof P. A. M. et al., 2010, A&A, 518, L137
Vicini B., Natta A., Marconi A., Testi L., Hollenbach D., Draine B. T., 1999, A&A, 342, 823
Werner M. W. et al., 2004, ApJS, 154, 1
Zhen J., Castellanos P., Paardekooper D. M., Ligterink N., Linnartz H., Nahon L., Joblin C., Tielens A. G. G. M., 2015, ApJ, 804, L7

This paper has been typeset from a TEX/LATEX file prepared by the author.